

# Evaluation of high-resolution predictions of fine particulate matter and its composition in an urban area using PMCAMx-v2.0

Brian T. Dinkelacker<sup>1</sup>, Pablo Garcia Rivera<sup>1</sup>, Ioannis Kioutsioukis<sup>2</sup>, Peter J. Adams<sup>3,4</sup>, Spyros N. Pandis<sup>5,6</sup>

<sup>1</sup>*Department of Chemical Engineering, Carnegie Mellon University, Pittsburgh, PA 15213, USA*

<sup>2</sup>*Department of Physics, University of Patras, 26500, Patras, Greece*

<sup>3</sup>*Department of Civil and Environmental Engineering, Carnegie Mellon University, Pittsburgh, PA 15213, USA*

<sup>4</sup>*Department of Engineering and Public Policy, Carnegie Mellon University, Pittsburgh, PA 15213, USA*

<sup>5</sup>*Institute of Chemical Engineering Sciences (FORTH/ICE-HT), 26504, Patras, Greece*

<sup>6</sup>*Department of Chemical Engineering, University of Patras, 26500, Patras, Greece*

\*Correspondence to: Spyros N. Pandis (spyros@chemeng.upatras.gr)

## Abstract

Accurately predicting urban PM<sub>2.5</sub> concentrations and composition has proved challenging in the past, partially due to the resolution limitations of computationally intensive chemical transport models (CTMs). Increasing the resolution of PM<sub>2.5</sub> predictions is desired to support emissions control policy development and address issues related to environmental justice. A nested grid approach using the CTM PMCAMx-v2.0 was used to predict PM<sub>2.5</sub> at increasing resolutions of 36 x 36, 12 x 12, 4 x 4, and 1 x 1 km for a domain largely consisting of Allegheny County and the city of Pittsburgh in southwestern Pennsylvania, US during February and July 2017. Performance of the model in reproducing PM<sub>2.5</sub> concentrations and composition was evaluated at the finest scale using measurements from regulatory sites as well as a network of low-cost monitors. Novel surrogates were developed to allocate emissions from cooking and on-road traffic sources to the 1 x 1 km resolution grid. Total PM<sub>2.5</sub> mass is reproduced well by the model during the winter period with low fractional error (0.3) and fractional bias (+0.05) when compared to regulatory measurements. Comparison with speciated measurements during this period identified small underpredictions of PM<sub>2.5</sub> sulfate, elemental carbon (EC), and organic aerosol (OA) offset by a larger overprediction of PM<sub>2.5</sub> nitrate. In the summer period, total PM<sub>2.5</sub> mass is underpredicted due to a large underprediction of OA (bias = -1.9 μg m<sup>-3</sup>, fractional bias

37 = -0.41). In the winter period, the model performs well reproducing the variability between  
38 urban measurements and rural measurements of local pollutants such as EC and OA. This  
39 effect is less consistent in the summer period due to a larger fraction of long range transport  
40 OA. Comparison with total  $PM_{2.5}$  concentration measurements from low-cost sensors  
41 showed improvements in performance with increasing resolution. Inconsistencies in  $PM_{2.5}$   
42 nitrate predictions in both periods are believed to be due to errors in partitioning between  
43  $PM_{2.5}$  and  $PM_{10}$  modes and motivate improvements to the treatment of dust particles within  
44 the model. The underprediction of summer OA would likely be improved by updates to  
45 biogenic SOA chemistry within the model, which would result in an increase of long-range  
46 transport SOA seen in the inner modeling domain. These improvements are obvious topics  
47 for future work towards model improvement. Comparison with regulatory monitors  
48 showed that increasing resolution from 36 km to 1 km improved both fractional error and  
49 fractional bias in both modeling periods. Improvements at all types of measurement  
50 locations indicated an improved ability of the model to reproduce urban-rural  $PM_{2.5}$   
51 gradients at higher resolutions.

52

## 53 **1 Introduction**

54 Fine particulate matter with aerodynamic diameter less than  $2.5 \mu m$  ( $PM_{2.5}$ ) has  
55 been associated with public health concerns due to short and long-term exposure. Some of  
56 the health effects of  $PM_{2.5}$  include increased risk of heart disease, increased likelihood of  
57 heart attacks and strokes, impaired lung development, and increased risk of lung disease  
58 (Dockery and Pope, 1994). Chemical transport models are frequently used for supporting  
59 the development of air quality policies designed to protect public health. To evaluate these  
60 policies, CTMs must simulate  $PM_{2.5}$  concentrations and their response to changes in  
61 emissions accurately.

62 Grid resolution is an important factor for CTM studies focusing on major urban  
63 areas since on-road traffic, commercial cooking, and biomass burning can have sharp  
64 gradients at the urban scale (Lanz et al., 2007; Allan et al., 2010). High spatial resolution  
65 measurements of  $PM_1$  in the city of Pittsburgh in high source-impact locations are on  
66 average 40% higher than at urban background locations (Gu et al., 2018). Heightened  
67 organic aerosol concentrations have been observed in commercial districts containing

68 multiple restaurants (Robinson et al., 2018). The demographic characteristics of the  
69 population can also have large variations at the neighborhood scale. High resolution  
70 predictions of pollutant concentrations allow for exposure assessments that compare  
71 subpopulations within the same metropolitan area to answer environmental justice related  
72 questions (Anand, 2002). The benefits of high-resolution modeling must be balanced with  
73 the increased complexity in the development of accurate, high-resolution emission  
74 inventories and increased computational cost and storage requirements.

75 Previous studies have found small to modest improvements on the predictive ability  
76 of regional CTMs for ozone in the summers of 1995, 1996, and 1997 moving from 36 km  
77 to 12 km resolution (Arunachalam et al., 2006) as well as in July 1988 using a dynamic  
78 grid system with sizes varying from 18.5 km to 4.625 km (Kumar and Russell, 1996).  
79 Stroud et al. (2011) found that the accurate simulation of urban and large industrial plumes  
80 required a grid resolution of 2.5 km in order to properly capture contributions from local  
81 sources of primary organic aerosol (POA) and volatile organic compounds (VOCs).  
82 Zakoura and Pandis (2019) investigated the effect of increasing grid resolution on PM<sub>2.5</sub>  
83 nitrate predictions and found that increasing the resolution to 4 km reduced bias by 65%.  
84 Fountoukis et al. (2013) reported a reduction of the bias for black carbon (BC)  
85 concentrations in the northeastern US when the grid resolution was reduced from 36x36  
86 km to 4x4 km. Pan et al., (2017) allocated county-based emissions at 4 km and 1 km grid  
87 resolution using the default approach from the National Emissions Inventory and found  
88 small changes in model performance for NO<sub>x</sub> and ozone. The 1 km simulation was able to  
89 resolve the detailed spatial variability of emissions in heavily polluted areas including  
90 highways, airports and industrially focused sub-regions.

91 One of the weaknesses of several of the above studies has been that the gridded  
92 emissions used at the higher resolutions were the results of interpolation. It is not clear if  
93 the remaining discrepancies between model predictions and measurements were due to  
94 errors in the spatial distribution of the high-resolution emissions, errors in the overall  
95 magnitude of the emissions over an urban area or other modeling errors in the simulation  
96 of various processes (chemistry, condensation/evaporation, etc.). It is also not clear if errors  
97 in previous simulations of urban PM<sub>2.5</sub> are due to inaccuracies in the transport of regional  
98 PM<sub>2.5</sub> to urban areas. In this work, we explore the impacts of increasing the resolution of

99 emissions inputs and CTM output on PM<sub>2.5</sub> predictions in southwestern Pennsylvania  
100 during the months of February and July 2017, including the ability of the model to  
101 reproduce observed differences between urban and rural PM<sub>2.5</sub> at the various grid  
102 resolutions.

103 Garcia Rivera et al. (2022) investigated the effects of increasing grid resolution of  
104 model inputs and CTM output on source resolved predictions of PM<sub>2.5</sub> concentration and  
105 population exposure at 36 km, 12 km, 4 km, and 1 km. Moving to 12 x 12 km resolution  
106 resolved much of the urban-rural gradient. Increasing to 4 x 4 km resolved stationary  
107 sources such as power plants and the 1 x 1 km resolution results revealed intra-urban  
108 variations and individual roadways. Regional pollutants with low spatial variability such  
109 as PM<sub>2.5</sub> nitrate showed modest changes when increasing the resolution to 4 x 4 km and  
110 higher. Local pollutants such as black carbon and organic aerosol showed gradients that  
111 were only resolved at the finest resolution. The ability of these simulations to reproduce  
112 PM<sub>2.5</sub> concentrations at different resolutions is evaluated here against multiple  
113 measurement sources and types. The two months of February and July 2017 were chosen  
114 to maximize the information gained with regard to the effects of seasonal variability of  
115 major emissions sources and meteorology on predicted concentrations while keeping the  
116 resources required for emissions inventory development at a feasible level.

117 We apply the Particulate Matter Comprehensive Air quality Model with Extensions  
118 version 2.0 (PMCAMx-v2.0) to study the impact of increasing model resolution on the  
119 ability to reproduce observed PM<sub>2.5</sub> concentrations. We evaluate the PMCAMx predictions  
120 at various grid resolutions against regulatory measurements of PM<sub>2.5</sub> concentration and  
121 composition, as well as measurements from a network of low-cost sensors (Zimmerman et  
122 al., 2018) during February and July 2017 which provide a unique opportunity for  
123 comparison not available to previous studies. Aerosol mass spectrometer (AMS)  
124 measurements taken in Pittsburgh during February 2017 were also used to evaluate model  
125 predictions.

126

## 127 **2 Model Description**

128 PMCAMx-v2.0, the Particulate Matter Comprehensive Air Quality Model with  
129 Extensions (Karydis et al., 2010; Murphy and Pandis, 2010; Tsimpidi et al., 2010) is a

130 state-of-the-art atmospheric chemical transport model (CTM) that uses the framework of  
131 the CAMx model (ENVIRON, 2005) with advanced aerosol chemistry modules. This  
132 model uses detailed emissions and meteorology inputs to dynamically predict changes in  
133 pollutant concentrations due to emission, transport, chemical reaction, removal processes,  
134 and aerosol processes. To track the dynamic evolution of aerosol mass, 10 moving size  
135 sections are used (Gaydos et al., 2003). The chemical mechanism SAPRC99 (Carter, 2000)  
136 was used for gas-phase chemistry, including 237 individual chemical reactions involving  
137 91 chemical species. Aqueous-phase chemistry is calculated with the Variable Size  
138 Resolution Model (Fahey and Pandis, 2001). PMCAMx-v2.0 considers the formation of  
139 aerosol mass comprised of sulfate, nitrate, ammonium, sodium, chloride, water, elemental  
140 carbon, as well as lumped organic species (both primary and secondary). Inorganic aerosol  
141 growth is modelled using an approach that assumes equilibrium between the bulk aerosol  
142 and gas phases. Partitioning of semivolatile inorganic aerosol is calculated using  
143 ISORROPIA-I (Nenes et al., 1998). The Volatility Basis Set (VBS) was used to calculate  
144 partitioning of organic aerosol components across a distribution of species volatility  
145 (Donahue et al., 2006). Volatility bins (10) with effective saturation concentration from  $10^{-3}$   
146  $^3$  to  $10^6 \mu\text{g m}^{-3}$  (at 298 K) are used for primary organic aerosol (POA). Secondary organic  
147 aerosol is split into anthropogenic (aSOA) and biogenic (bSOA) components, formed from  
148 a variety of SOA-forming volatile organic compounds (VOCs) from human activity and  
149 natural sources, respectively using  $\text{NO}_x$ -dependent SOA formation yields (Lane et al.,  
150 2008). Both aSOA and bSOA are split into 4 volatility bins with effective saturation  
151 concentration from  $10^0$  to  $10^3 \mu\text{g m}^{-3}$  (at 298 K).

152

### 153 **3 Model Application**

154 Air quality simulations of a 5184 km<sup>2</sup> area comprised of southwestern Pennsylvania  
155 and smaller parts of eastern Ohio and northern West Virginia were performed using  
156 PMCAMx. Two distinct simulation periods of February and July 2017 were investigated.  
157 The approach of Garcia et al. (2022) was used to produce speciated PM<sub>2.5</sub> concentration  
158 predictions at spatial resolution of 36 km, 12 km, 4 km, and 1 km. Surface-level boundary  
159 conditions for the 36 x 36 km simulations are provided in Table S1.

160 Meteorological fields were calculated using the Weather Research and Forecasting  
161 model (WRF-v3.6.1) with horizontal resolution of 12 x 12 km, providing wind  
162 components, eddy diffusivity, temperature, pressure, humidity, clouds, and precipitation  
163 inputs for use in PMCAMx. Meteorology initial and boundary conditions were retrieved  
164 from the ERA-Interim global climate re-analysis database. The United States Geological  
165 Survey database was used to obtain input data for terrain, land-use, and soil type. When  
166 necessary, WRF output was interpolated to higher resolutions. An evaluation of  
167 interpolated meteorological inputs using data from METAR stations near the city of  
168 Pittsburgh in southwestern Pennsylvania determined that errors in the magnitude and  
169 phasing of diurnal cycles of temperature, relative humidity, and wind speed are  
170 appropriately small for use in air quality studies. These results are provided in the  
171 supplementary material (Fig. S1, S2).

172 Anthropogenic emissions are derived from the 2017 projections of the 2011  
173 National Emissions Inventory (Eyth and Vukovich, 2015) modelling platform. The Sparse  
174 Matrix Operator Kernel Emissions modeling system (SMOKE) was used, along with  
175 meteorological inputs to calculate emissions at a horizontal resolution of 12 x 12 km.  
176 Default spatial surrogates were used to allocate these emissions to higher resolutions.  
177 Custom surrogates were developed for commercial cooking and on-road traffic emissions  
178 sectors within the 1 x 1 km grid and used for the primary analysis in this work. The use of  
179 these new surrogates results in different spatial distribution of emissions for cooking and  
180 on-road traffic sources than what would be observed with the default spatial surrogates.  
181 Additional simulations were performed to quantify the impact of these proposed surrogates  
182 on predicted PM<sub>2.5</sub> concentrations.

183 For commercial cooking, the normalized restaurant count was used to distribute the  
184 emissions from the sector in space within the 1 x 1 km domain. This surrogate distributed  
185 commercial cooking emissions based on the density of restaurants identified by the Google  
186 Places Application Programming Interface. To allocate on-road traffic emissions, the  
187 output from the traffic model of Ma et al. (2020) was used. This model simulates hourly  
188 traffic using data from the Pennsylvania Department of Transportation. Emissions from the  
189 on-road traffic sector were then allocated based on these values.

190 Model predictions of sulfate, nitrate, elemental carbon and organic aerosol were  
191 compared with measurements from 4 sites from the EPA Chemical Speciation Network  
192 (EPA-CSN) (U.S. EPA, 2002). The locations of these 4 sites are shown in Figure 1a. These  
193 sites include: Lawrenceville, an urban background site 4 km northeast of downtown  
194 Pittsburgh; Hillman State Park located in a state park in southwest Pennsylvania in a rural  
195 and remote location approximately 40 km upwind of Pittsburgh; Steubenville in the Ohio  
196 River Valley close to industrial installations and coal-fired power plants, and the Liberty-  
197 Clairton monitor, which is located close to the Clairton Coke Works in the Monongahela  
198 River Valley 14 km southeast of downtown Pittsburgh. Speciated PM<sub>2.5</sub> measurements  
199 from EPA-CSN sites are available every three days during the simulation periods. Daily  
200 non-speciated measurements of total PM<sub>2.5</sub> mass concentration are available from 17 sites  
201 within the inner simulation domain and are used to further evaluate total PM<sub>2.5</sub> mass  
202 concentration predictions. The locations of these sites are also shown in Figure 1a.

203 For February 2017, high-resolution AMS measurements from the Carnegie Mellon  
204 University supersite (Gu et al., 2018) are used to evaluate the predicted chemical  
205 composition of PM<sub>2.5</sub> model predictions. Positive matrix factorization results are also used  
206 to investigate the breakdown of organic aerosol components. AMS measurements were  
207 taken continuously from February 1 to February 14, 2017. Due to uncertainties with the  
208 AMS collection efficiency during this campaign, we use here only the fractional particle  
209 composition data.

210 PMCAMx predictions of PM<sub>2.5</sub> were also compared with measurements taken with  
211 a network of Real-time Affordable Multi-Pollutant (RAMP) monitors (Zimmerman et al.,  
212 2018) distributed in the city of Pittsburgh. During the winter period measurements at 7 sites  
213 were available, all located within the boundaries of the city of Pittsburgh, while 22 sites  
214 were in operation during the summer period with a few sites also outside the city (Fig. 1b).  
215 Uncertainty in these low-cost measurements of PM<sub>2.5</sub> mass concentration is between 3-4  
216  $\mu\text{g m}^{-3}$  for hourly averaging times (Malings et al., 2019).

217 The model performance is assessed in terms of the mean bias (BIAS), the mean  
218 error (ERROR), the fractional bias (FBIAS) and the fractional error (ERROR):

$$219 \quad \text{BIAS} = \frac{1}{N} \sum_{i=1}^N P_i - O_i \quad (1)$$

$$220 \quad \text{FBIAS} = \frac{2}{N} \sum_{i=1}^N \frac{P_i - O_i}{P_i + O_i} \quad (2)$$

$$221 \quad \text{ERROR} = \frac{1}{N} \sum_{i=1}^N |P_i - O_i| \quad (3)$$

$$223 \quad \text{FERROR} = \frac{2}{N} \sum_{i=1}^N \frac{|P_i - O_i|}{P_i + O_i} \quad (4)$$

222

224 where  $N$  is the number of valid measurements,  $P_i$  is the predicted concentration and  $O_i$  is  
 225 the corresponding observed concentration. The fractional error metric is bounded by 0  
 226 (perfect prediction performance) and 2.0 (extremely poor prediction performance).  
 227 Fractional bias is bounded by -2.0 (extreme underprediction) and +2.0 (extreme  
 228 overprediction).

229

## 230 **4 Evaluation of high-resolution model performance**

### 231 **4.1 Winter**

232 Table 1 summarizes the performance metrics of daily average PMCAMx-v2.0  
 233 PM<sub>2.5</sub> predictions in the 1x1 km resolution, when compared with daily measurements from  
 234 EPA regulatory PM<sub>2.5</sub> monitors. The speciated performance is illustrated in Figure 2.  
 235 Predictions of total PM<sub>2.5</sub> mass perform well against regulatory measurements in the  
 236 February simulation period, with fractional error of 0.3 and fractional bias of +0.07.

237 Average measured PM<sub>2.5</sub> sulfate for this time period was 1.9 μg m<sup>-3</sup>. Lower sulfate  
 238 levels were observed at the Lawrenceville site in Pittsburgh (1.2 μg m<sup>-3</sup>) while significantly  
 239 higher levels were observed at the Steubenville site (3.1 μg m<sup>-3</sup>). Predicted domain-average  
 240 PM<sub>2.5</sub> sulfate at 1 x 1 km resolution was 1.3 μg m<sup>-3</sup>. Overall fractional error for sulfate  
 241 predictions was 0.41 and no overall bias was observed (fractional bias of -0.02). PM<sub>2.5</sub>  
 242 sulfate was slightly overpredicted at Hillman State Park (+0.18 fractional bias) and  
 243 Lawrenceville (+0.25 fractional bias) and underpredicted at the industrial sites,  
 244 Steubenville (-0.24 fractional bias) and Liberty/Clairton (-0.43 fractional bias) where  
 245 observed PM<sub>2.5</sub> sulfate concentrations were higher.



246 Overpredictions were seen for PM<sub>2.5</sub> nitrate, with a fractional bias of +0.81. The  
247 average measured concentration at EPA-CSN sites within the simulation domain was 1.5  
248  $\mu\text{g m}^{-3}$ , while the domain-average predicted concentration was 1.8  $\mu\text{g m}^{-3}$ . Observed  
249 average PM<sub>2.5</sub> nitrate concentrations at Hillman State Park and Lawrenceville were slightly  
250 lower at 1.1  $\mu\text{g m}^{-3}$  and 1.2  $\mu\text{g m}^{-3}$ , respectively. Nitrate at the Steubenville location was  
251 observed to be higher on average at 2.2  $\mu\text{g m}^{-3}$ . This overprediction is seen at all sites but  
252 is particularly prevalent at Hillman State Park, Lawrenceville, and Liberty/Clairton, where  
253 errors are of the order of a factor of two. Previous PMCAMx modeling studies have found  
254 similar over-predictions. Part of this overprediction was due to the use of coarse-grid  
255 resolution (Zakoura and Pandis, 2018), but this is unlikely to be the cause here, because  
256 81% of the predicted domain-average nitrate is transported from outside of the inner  
257 modeling domain. These inconsistencies in PM<sub>2.5</sub> nitrate predictions are likely due to errors  
258 in the partitioning of nitrate between the fine (PM<sub>2.5</sub>) and coarse (PM<sub>10</sub>) modes, resulting  
259 in an overprediction of PM<sub>2.5</sub> nitrate. Resolving this modeling error likely requires  
260 improvements to the treatment of dust within the model, and the use of a dynamic approach  
261 for inorganic aerosol calculations rather than the bulk equilibrium approach.

262 The behavior of PM<sub>2.5</sub> ammonium measurements is similar to that of nitrate as most  
263 of it is in the form of ammonium nitrate. The average measured concentration at the four  
264 EPA-CSN stations was 0.9  $\mu\text{g m}^{-3}$ . At Hillman State Park and Lawrenceville, the measured  
265 average was lower at 0.5  $\mu\text{g m}^{-3}$  but higher at the Liberty/Clairton location at 2.1  $\mu\text{g m}^{-3}$ .  
266 PM<sub>2.5</sub> ammonium was overpredicted similarly to PM<sub>2.5</sub> nitrate with +0.83 fractional bias.  
267 The average measured concentration of PM<sub>2.5</sub> elemental carbon at EPA-CSN sites during  
268 February 2017 was 1.1  $\mu\text{g m}^{-3}$ . Elemental carbon concentrations are more localized than  
269 the inorganic PM<sub>2.5</sub> components. At Hillman State Park the average measured  
270 concentration was only 0.5  $\mu\text{g m}^{-3}$  while at Liberty/Clairton the averaged measured  
271 concentration was 2.9  $\mu\text{g m}^{-3}$ . For elemental carbon, the predicted domain-average was 0.4  
272  $\mu\text{g m}^{-3}$ . Average elemental carbon concentration in the 4 x 4 km simulation grid outside of  
273 the inner modeling domain was 0.3  $\mu\text{g m}^{-3}$ . Black carbon predictions at all sites had a  
274 fractional error of 0.71 with fractional bias of -0.08. Elemental carbon was overpredicted  
275 at the urban site with fractional bias of 0.73 and underpredicted at the other sites.

276 Average measured OA during this period was  $4.4 \mu\text{g m}^{-3}$ , but with significant  
277 spatial variability. At Hillman State Park and Lawrenceville measured OA was  $3.1 \mu\text{g m}^{-3}$   
278 and  $3.4 \mu\text{g m}^{-3}$ , respectively. At Liberty/Clairton and Steubenville the average measured  
279 OA was  $7 \mu\text{g m}^{-3}$  and  $6.3 \mu\text{g m}^{-3}$ , respectively. Domain-average predicted OA was  $2.2 \mu\text{g}$   
280  $\text{m}^{-3}$ . Outside of the inner 1 x 1 km domain, average predicted OA was  $1.6 \mu\text{g m}^{-3}$ ,  
281 suggesting that the majority of predicted OA is transported from outside of the 1 x 1 km  
282 grid. Overall OA prediction performance in the winter is acceptable at 0.53 fractional error  
283 and low fractional bias (-0.01). At individual sites, performance varies. OA is predicted  
284 with low fractional bias (-0.10) at the rural Hillman State Park site. OA is overpredicted by  
285 with +0.31 fractional bias at the urban site in Lawrenceville and underpredicted at both  
286 industrial sites. An added degree of uncertainty exists with the industrial sites within the  
287 inner domain. The emissions from these sources may be underestimated in the inventory  
288 and these locations are also difficult to accurately model due to their geographic location  
289 in river valleys.

290 Average concentrations of  $\text{PM}_{2.5}$  sulfate, nitrate, and ammonium in the 4 x 4 km  
291 resolution domain were around 83% of the average predicted concentrations in the inner 1  
292 x 1 km simulation grid. For elemental carbon and OA, the outer concentration was 64%  
293 and 73% of the inner concentration respectively, indicating that these species had  
294 significant local sources. For these more local pollutants, the model appears to perform  
295 well in terms of capturing urban-rural gradients, but with a tendency towards  
296 underprediction at the rural site in Hillman State Park and overprediction at the urban site  
297 in Lawrenceville. The model also underpredicts EC and OA at the industrial locations,  
298 especially elemental carbon (-0.67 and -1.02 fractional bias at Steubenville and  
299 Liberty/Clairton, respectively). This again suggests errors in the emissions inventory or  
300 problems in simulating atmospheric dispersion near the sources.

301 Comparisons with the  $\text{PM}_1$  composition as determined by the AMS from February  
302 3 through February 14, 2017, show excellent agreement for all species (Fig. 3a). Gu et al.  
303 (2018) used PMF analysis and allocated total measured OA into five factors. Three of them  
304 corresponded to primary organic aerosol: hydrocarbon-like OA (HOA), cooking OA  
305 (COA) and biomass burning OA (BBOA) and two secondary OA factors: more-oxidized  
306 organic aerosol (MO-OOA) and less-oxidized organic aerosol (LO-OOA). To compare

307 PMCAMx predictions with the primary PMF factors, two additional simulations were  
308 performed in which emissions from biomass burning and commercial cooking were set to  
309 zero. The predicted concentrations were then subtracted from the base case to estimate the  
310 contribution from each respective source. The remaining primary OA was assigned to  
311 HOA. The LO-OOA and MO-OOA factors were added together and compared with the  
312 PMCAMx SOA predictions.

313 The predicted cooking OA (COA) at the CMU site is 25% of the total OA and is in  
314 agreement with the PMF/AMS estimate of 22% (Fig. 3b). This is encouraging given the  
315 small bias of the model for total OA levels. The predicted HOA and BBOA are higher than  
316 measured by a factor of 2 or more. At the same time, the measurements indicate a  
317 surprisingly high contribution of SOA (53% of the total OA) during a period with little  
318 photochemical activity and low levels of OH radicals. SOA is predicted to be just 20% of  
319 the total during this time period. These discrepancies may indicate transformation of the  
320 HOA and BBOA to OOA during this wintertime period, that are not included in the model.  
321 Kodros et al. (2020) recently suggested that BBOA can react with the  $\text{NO}_3$  radical during  
322 the winter and can be transformed to OOA.

323

## 324 **4.2 Summer**

325 Total  $\text{PM}_{2.5}$  mass concentrations are underpredicted in the summer period. The  
326 average measured  $\text{PM}_{2.5}$  value in the regulatory network in the area was  $11.4 \mu\text{g m}^{-3}$ , while  
327 the average predicted value at the regulatory sites was  $4 \mu\text{g m}^{-3}$  lower.

328 Speciated  $\text{PM}_{2.5}$  performance is illustrated in Figure 4. Average measured  $\text{PM}_{2.5}$   
329 sulfate for the summer period was  $2 \mu\text{g m}^{-3}$ . Slightly lower levels were observed at the  
330 Lawrenceville site in Pittsburgh ( $1.9 \mu\text{g m}^{-3}$ ). Liberty/Clairton had higher measured sulfate  
331 concentrations ( $2.6 \mu\text{g m}^{-3}$ ), but this difference between locations is lower than what was  
332 observed in the winter period. Predicted domain-average  $\text{PM}_{2.5}$  sulfate at  $1 \times 1 \text{ km}$   
333 resolution was  $1.3 \mu\text{g m}^{-3}$ . Overall fractional error (0.62) and fractional bias (-0.21) for  
334 sulfate predictions was higher than in the winter simulation period.  $\text{PM}_{2.5}$  sulfate was  
335 underpredicted at all sites but to the largest extent at Hillman State Park (-0.36 fractional  
336 error).

337 Overpredictions of PM<sub>2.5</sub> nitrate were also seen in the summer period, and at all  
338 types of sites. Average measured PM<sub>2.5</sub> nitrate was 0.3 μg m<sup>-3</sup>, much lower than in the  
339 winter. The domain-average predicted PM<sub>2.5</sub> nitrate was 0.7 μg m<sup>-3</sup>. Again, predicted PM<sub>2.5</sub>  
340 nitrate in the inner domain is dominated by material transported from outside the  
341 boundaries (75%), so the issue is not resolved by using a high-resolution grid.  
342 Improvements to PM<sub>2.5</sub> nitrate formation are needed in the form of dust models with  
343 increased complexity to resolve the issues with fine-coarse mode partitioning of particulate  
344 nitrate. These issues have been highlighted by decreased concentrations of PM<sub>2.5</sub> pollution  
345 in recent years.

346 Observed PM<sub>2.5</sub> ammonium concentrations at EPA-CSN sites were also much  
347 lower in the summer with an average value of 0.5 μg m<sup>-3</sup>. Slightly higher average  
348 concentrations were observed at Liberty/Clairton (0.7 μg m<sup>-3</sup>) and slightly lower  
349 concentrations were observed at Steubenville (0.4 μg m<sup>-3</sup>). The domain-average predicted  
350 PM<sub>2.5</sub> ammonium concentration was 0.6 μg m<sup>-3</sup>. The average concentration directly outside  
351 of the inner domain was 0.5 μg m<sup>-3</sup>. Overall performance was better for ammonium in the  
352 summer than in the winter with fractional error of 0.62 and fractional bias of +0.44. The  
353 strongest overprediction is seen at the Steubenville site (+0.57 fractional bias).

354 The average measured elemental carbon (EC) concentration in July was 0.7 μg  
355 m<sup>-3</sup>. Measured EC carbon was significantly higher at Liberty/Clairton (1 μg m<sup>-3</sup>) and lower  
356 at rural Hillman State Park (0.4 μg m<sup>-3</sup>). Domain-average predicted EC was 0.3 μg m<sup>-3</sup>.  
357 Outside of the inner domain, the average predicted concentration was 0.2 μg m<sup>-3</sup>. Elemental  
358 carbon predictions in July had a lower fractional error compared to the winter at 0.60 but  
359 showed a stronger negative fractional bias at -0.33. The model severely underpredicts at  
360 Hillman State Park (-0.86 fractional bias), where measured concentrations were lowest, but  
361 also at the industrial sites of Steubenville (-0.55 fractional bias) and Liberty/Clairton (-0.65  
362 fractional bias). EC was slightly overpredicted at the urban Lawrenceville location (+0.14  
363 fractional bias). While the urban-rural gradient in EC is slightly overpredicted, the model  
364 is still able to capture well the variability between rural (Hillman State Park) and urban  
365 (Lawrenceville). The model struggles to reproduce high measurements of EC at the  
366 Steubenville site, reiterating the issues with industrial EC seen in the winter.

367 Average measured OA concentration was  $4.5 \mu\text{g m}^{-3}$  in July. Higher concentrations  
368 were observed at the industrial sites, Liberty/Clairton and Steubenville ( $5.0 \mu\text{g m}^{-3}$ )  
369 respectively. The lowest observed concentration was in Hillman State Park ( $3.6 \mu\text{g m}^{-3}$ ).  
370 The average predicted concentration at CSN sites was  $2.7 \mu\text{g m}^{-3}$ . On average, OA is  
371 underpredicted with fractional bias of -0.47. This underprediction occurs at all sites but is  
372 less prevalent at the urban Lawrenceville location (-0.19 fractional bias) and is most  
373 dramatic in Steubenville (-0.65 fractional bias). Because such a large fraction of the OA in  
374 the summer is predicted to be secondary (50% of local OA on average) and transported  
375 from outside of the inner modeling domain (84% of total OA), treatment of SOA formation  
376 is likely a key factor contributing to the underprediction of  $\text{PM}_{2.5}$  in the summer. While  
377 these improvements are necessary for overall model improvement, they do not have  
378 significant impact on the urban-rural gradients which are the focus of this work and are  
379 driven by primary species. The performance of EC predictions in various locations is  
380 encouraging with regard to primary  $\text{PM}_{2.5}$  performance.

381

## 382 **5 Effect of grid resolution on $\text{PM}_{2.5}$ performance**

383 To determine the effect of grid resolution on the ability of the model to resolve  
384 geographical variations in  $\text{PM}_{2.5}$  concentrations, daily average measurements from the 17  
385 EPA regulatory sites were compared with PMCAMx predictions from simulations at 36  
386 km, 12 km, 4 km and 1 km. The PMCAMx performance metrics are summarized in Table  
387 2.

388

### 389 **5.1 Winter**

390 During the winter period, increasing grid resolution reduces the average fractional  
391 error from 34% at 36 x 36 km to 30% at 1 x 1 km. The higher resolution also improved the  
392 fractional bias, from -0.09 at 36 x 36 km to +0.05 at 1 x 1 km. The performance is illustrated  
393 in Figure 5. Performance at urban locations stayed steady in the winter, with fractional  
394 error changing from 0.30 to 0.26 and fractional bias changing from +0.02 to +0.08 moving  
395 from 36 km to 1 km resolution (Fig. S3). Rural performance improved to a greater extent,  
396 with fractional error improving from 0.33 to 0.28 and fractional bias lowering from +0.21  
397 to +0.11.

398 The comparison with low-cost sensor measurements largely represents the  
399 performance of the model in terms of urban PM<sub>2.5</sub> predictions. The performance metrics of  
400 PMCAMx-v2.0 when compared to measurements from low-cost sensors are shown in  
401 Table 3. Moving from low to high resolution, the predictions go from no bias (-0.02) to a  
402 bias of +0.24. Due to the slight overprediction of the urban-rural gradient seen earlier  
403 (particularly with EC), the high resolution would likely lead to more positive biases when  
404 compared to a largely urban network. Fractional error increases slightly, but still exhibits  
405 good performance moving from 0.33 to 0.37.

406

## 407 **5.2 Summer**

408 In the summer period, (Fig. 6) the model performance improved as the resolution  
409 increased from 36 km to 1 km. Fractional error decreased from 0.53 to 0.48, while  
410 fractional bias increased from -0.46 to -0.39. In July, performance at the urban locations  
411 significantly increased with resolution (Fig. S4). Fractional error decreased from 52% at  
412 36 x 36 km to 0.42 at 1 x 1 km. Fractional bias also improved from -0.46 at the coarse grid  
413 resolution to -0.39 at the finest scale. Rural predictions of PM<sub>2.5</sub> were also better with  
414 increasing resolution in the summer. Fractional error decreased from 0.31 to 0.22 while  
415 fractional bias decreased from +0.05 to -0.05.

416 Larger improvements are seen with increasing resolution during the summer when  
417 compared to measurements from low-cost sensors. Starting from a large negative bias of  
418  $-5.4 \mu\text{g m}^{-3}$  (fractional bias of -0.48) at the 36 x 36 km resolution, performance consistently  
419 improved with each increasing resolution step with the bias eventually reaching  $-3.7 \mu\text{g}$   
420  $\text{m}^{-3}$  (fractional bias of -0.27) at the 1 x 1 km. There was also a reduction in fractional error  
421 from 0.52 at the coarse to 0.41 at the fine 1 x 1 km resolution. These metrics are  
422 encouraging, although they are likely impacted by an overprediction of the urban-rural  
423 gradient, similar to winter. Improvement of the secondary PM<sub>2.5</sub> predictions is still the  
424 largest source of error between predictions and this source of measurements.

425

## 426 **6 Evaluation of Novel Emissions Surrogates**

427 For commercial cooking, the normalized restaurant count was used to distribute the  
428 emissions from the sector in space within the 1 x 1 km domain. Geographical information

429 was collected for all restaurant locations in the inner domain from the Google Places  
430 Application Programming Interface. This includes southwestern Pennsylvania as well as  
431 parts of eastern Ohio and northern West Virginia. To allocate on-road traffic emissions, the  
432 output from the traffic model of Ma et al. (2020) was used. This model simulated hourly  
433 traffic using data from the Pennsylvania Department of Transportation sites located  
434 throughout the inner modeling domain. The use of new surrogates resulted in a new spatial  
435 distribution of emissions for both cooking and onroad traffic sources when compared to  
436 those developed using default emissions surrogates. The changes in spatial distributions  
437 are illustrated in the supplementary material (Figures S5, S6, S7, and S8). These novel  
438 emissions surrogates resulted in larger emissions of both traffic and cooking in the  
439 downtown area. In the case of on-road traffic, major highways in the inner domain are  
440 emphasized with the new surrogates.

441 For both February and July 2017, the largest observed change when using the novel  
442 surrogates is an increase in predicted  $PM_{2.5}$  of around  $3 \mu g m^{-3}$  in the downtown Pittsburgh  
443 area (Fig. 7). Differences in predicted  $PM_{2.5}$  concentrations outside of the urban areas of  
444 the inner domain are very small (less than  $0.5 \mu g m^{-3}$  in magnitude).

445 Model performance at 1 x 1 km resolution is detailed in Table 4. Negligible changes  
446 in performance were seen using EPA regulatory  $PM_{2.5}$  data in February 2017. Small  
447 improvements were seen at regulatory sites in July 2017, where fractional error was  
448 reduced from 51% to 48% and fractional bias increased from -43% to -39%. A positive  
449 shift in fractional bias was seen with the use of the new surrogates during both periods  
450 when compared to low-cost sensor measurements, resulting in a modest overprediction of  
451  $PM_{2.5}$  in the winter (+0.24 fractional bias) and a modest underprediction of  $PM_{2.5}$  in the  
452 summer (-0.27 fractional bias). The larger changes when compared to the low-cost sensor  
453 measurements are a result of the location of the low-cost sensors in urban areas, where the  
454 new surrogates predicted elevated  $PM_{2.5}$  mass concentrations.

## 455 **7 Conclusions**

456 We applied PMCAMx-v2.0 over southwestern Pennsylvania during February and  
457 July 2017 at grid resolutions of 36 km, 12 km, 4 km and 1 km. Emissions were calculated  
458 for the relevant grids by using the spatial surrogates provided along with the 2011 NEI for

459 all emissions sectors except traffic and cooking, for which 1 x 1 km spatial surrogates were  
460 developed.

461 PMCAMx predicts winter sulfate, elemental carbon and organic aerosol  
462 concentrations with fractional biases below 10% at high resolution. Nitrate concentrations  
463 are overpredicted (bias +1.4  $\mu\text{g m}^{-3}$ ) following the trend of previous studies in both the US  
464 and Europe. Agreement with total  $\text{PM}_{2.5}$  measurements is also encouraging with a  
465 fractional bias of +5%. Variability between urban and rural predictions of local pollutants  
466 EC and organic aerosol (OA) are reproduced well in the winter period. Underpredictions  
467 of summer OA concentrations led to underpredictions of total  $\text{PM}_{2.5}$  mass. Summer sulfate  
468 is reproduced with fractional bias of -21% and elemental carbon (EC) is predicted with  
469 fractional bias of -33%. Nitrate is similarly overpredicted in the summer with fractional  
470 bias of +70% although with a much smaller magnitude than in the winter (+0.4  $\mu\text{g m}^{-3}$ ).  
471 Differences between urban and rural EC is also predicted well in the summer, while OA is  
472 predicted to vary little between urban and rural locations. This is indicative of a greater  
473 contribution of secondary species to OA during this period.

474  $\text{PM}_{2.5}$  prediction performance improved in almost all cases when increasing  
475 the resolution from 36 km to 1 km. Underpredictions at urban sites and overpredictions at  
476 rural sites were reduced at the same time. This is true when comparing against  
477 measurements from regulatory sites as well as low-cost monitors. The improved  
478 performance here is evidence of the enhanced ability of the model to capture important  
479 urban-rural gradients in  $\text{PM}_{2.5}$  pollution by increasing the resolution of predictions to 1 x 1  
480 km. Increasing resolution of predictions has been shown here to improve model  
481 performance when comparing predicted  $\text{PM}_{2.5}$  concentrations with observations from  
482 regulatory monitors and low-cost sensors. However, these simulations highlight the need  
483 for specific improvements to some of the secondary  $\text{PM}_{2.5}$  formation pathways in the  
484 model. Improvement of the treatment of dust in the model is required to better model the  
485 distribution of particulate nitrate between  $\text{PM}_{2.5}$  and  $\text{PM}_{10}$  modes. Additionally,  
486 improvements to SOA formation chemistry within the model, particularly from biogenic  
487 sources outside of the inner modeling domain, will likely have a significant impact on  
488  $\text{PM}_{2.5}$  predictions around the city of Pittsburgh.

489



490

491 *Code Availability.* The PMCAMx-v2.0 code is available in Zenodo at  
492 <https://doi.org/10.5281/zenodo.6772851> (Dinkelacker et al., 2022). License (for files):  
493 GNU General Public License v3.0.

494

495 *Author contributions.* BTD performed the PMCAMx simulations, analyzed the results, and  
496 wrote the manuscript. PGR wrote the code for data analysis, prepared anthropogenic  
497 emissions and other inputs for the PMCAMx simulations, and assisted in writing the  
498 manuscript. IK set up the WRF simulations and assisted in the preparation of the  
499 meteorological inputs. SNP and PJA designed and coordinated the study and helped in the  
500 writing of the paper. All authors reviewed and commented on the manuscript.

501

502 *Competing Interests.* The authors declare that they have no conflict of interest.

503 *Financial support.* This work was supported by the Center for Air, Climate, and Energy  
504 Solutions (CACES) which was supported under Assistance Agreement No. R835873  
505 awarded by the U.S. Environmental Protection Agency and the Horizon-2020 Project  
506 REMEDIA of the European Union under grant agreement No 874753.

507

## 508 **References**

509 Allan, J. D.; Williams, P. I.; Morgan, W. T.; Martin, C. L.; Flynn, M. J.; Lee, J.; Nemitz,  
510 E.; Phillips, G. J.; Gallagher, M. W.; Coe, H.: Contributions from transport, solid  
511 fuel burning and cooking to primary organic aerosols in two UK cities, *Atmos.*  
512 *Chem. Phys.*, 10, 647-668. doi:10.5194/acp-10-647-2010, 2010.

513 Anand, S.: The concern for equity in health, *JECH*, 56, 485–487.  
514 doi:10.1136/jech.56.7.485, 2002.

515 Arunachalam, S., Holland, A., Do, B., Abraczinskas, M.: A quantitative assessment of the  
516 influence of grid resolution on predictions of future-year air quality in North  
517 Carolina, USA, *Atmos. Environ.*, 40, 5010–5026.  
518 doi:10.1016/j.atmosenv.2006.01.024, 2006.

519 Carter, W.P.L.: Documentation of the SAPRC-99 chemical mechanism for VOC reactivity  
520 assessment: Final report to California Air Resources Board, Contract 92-329 and

521 Contract 95-308, California Air Resources Board, Sacramento, California, 2000.

522 Dinkelacker, B.T., Garcia Rivera, P., Kioutsioukis, I., Adams, P., Pandis, S.N.: Source  
523 Code for PMCAMx-v2.0: "High-resolution modeling of fine particulate matter in  
524 an urban area using PMCAMx-v2.0", Zenodo [model code], [https://doi.org/  
525 10.5281/zenodo.7358180](https://doi.org/10.5281/zenodo.7358180), 2022.

526 Dockery, D.W., Pope, C.A.: Acute Respiratory Effects of Particulate Air Pollution, *Annu.  
527 Rev. Public Health*, 15, 107–132. doi:10.1146/annurev.pu.15.050194.000543,  
528 1994.

529 Donahue, N.M., Robinson, A.L., Stanier, C.O., Pandis, S.N.: Coupled partitioning,  
530 dilution, and chemical aging of semivolatile organics, *Environ. Sci. Technol.*, 40,  
531 2635–2643. doi:10.1021/es052297c, 2006.

532 ENVIRON: CAMx (Comprehensive Air Quality Model with Extensions) User's Guide  
533 Version 4.20, 2005.

534 Eyth, A., Vukovich, J.: Technical Support Document (TSD): Preparation of emissions  
535 inventories for the version 6.2, 2011 emissions modeling platform., 2015.

536 Fahey, K. M.; Pandis, S. N.: Optimizing model performance: variable size resolution in  
537 cloud chemistry modeling, *Atmos. Environ.*, 35, 4471-4478, doi:10.1016/S1352-  
538 2310(01)00224-2, 2001.

539 Fountoukis, C., Koraj, D., Denier van der Gon, H.A.C., Charalampidis, P.E., Pilinis, C.,  
540 Pandis, S.N.: Impact of grid resolution on the predicted fine PM by a regional 3-D  
541 chemical transport model, *Atmos. Environ.*, 68, 24–32.  
542 doi:10.1016/j.atmosenv.2012.11.008, 2013.

543 Garcia Rivera, P., Dinkelacker, B. T., Kioutsioukis, I., Adams, P. J., and Pandis, S. N.:  
544 Source-resolved variability of fine particulate matter and human exposure in an  
545 urban area, *Atmos. Chem. Phys.*, 22, doi:10.5194/acp-22-2011-2022, 2022.

546 Gaydos, T.M.; Koo, B.; Pandis, S.N.; Chock, D.P.: Development and application of an  
547 efficient moving sectional approach for the solution of the atmospheric aerosol  
548 condensation/evaporation equations, *Atmos. Environ.*, 37, 3303-3316,  
549 doi:10.1016/S1352-2310(03)00267-X, 2003.

550 Gu, P., Li, H.Z., Ye, Q., Robinson, E.S., Apte, J.S., Robinson, A.L., Presto, A.A.: Intracity  
551 variability of particulate matter exposure is driven by carbonaceous sources and

552 correlated with land-use variables, *Environ. Sci. Technol.*, 52, 11545–11554.  
553 doi:10.1021/acs.est.8b03833, 2018.

554 Karydis, V.A., Tsimpidi, A.P., Fountoukis, C., Nenes, A., Zavala, M., Lei, W., Molina,  
555 L.T., Pandis, S.N.: Simulating the fine and coarse inorganic particulate matter  
556 concentrations in a polluted megacity, *Atmos. Environ.*, 44, 608–620.  
557 doi:10.1016/j.atmosenv.2009.11.023, 2010.

558 Kodros, J.K., Papanastasiou, D.K., Paglione, M., Masiol, M., Squizzato, S., Florou, K.,  
559 Skyllakou, K., Kaltsonoudis, C., Nenes, A., Pandis, S.N.: Rapid dark aging of  
560 biomass burning as an overlooked source of oxidized organic aerosol, *Proc. Natl.*  
561 *Acad. Sci.*, 117 (52), 33028-33033, doi:10.1073/pnas.2010365117, 2020.

562 Kumar, N., Russell, A.G.: Multiscale air quality modeling of the Northeastern United  
563 States, *Atmos. Environ.*, 30, 1099–1116. doi:10.1016/1352-2310(95)00317-7,  
564 1996.

565 Lane, T.E., Donahue, N.M., Pandis, S.N.: Effect of NO<sub>x</sub> on secondary organic aerosol  
566 concentrations, *Environ. Sci. Technol.*, 42, 6022–6027. doi:10.1021/es703225a,  
567 2008.

568 Lanz, V. A.; Alfarra, M. R.; Baltensperger, U.; Buchmann, B.; Hueglin, C.; Prevot, A. S.  
569 H.: Source apportionment of submicron organic aerosols at an urban site by factor  
570 analytical modelling of aerosol mass spectra, *Atmos. Chem. Phys.*, 7, 1503-1522.  
571 doi:10.5194/acp-7-1503-2007, 2007.

572 Ma, W., Pi, X., Qian, S.: Estimating multi-class dynamic origin-destination demand  
573 through a forward-backward algorithm on computational graphs. *Transportation*  
574 *Research Part C: Emerging Technologies*, 119, 102747, doi:10.1016/j.trc.2020.  
575 102747, 2020.

576 Malings, C., Tanzer, R., Haurlyiuk, A., Saha, P.K., Robinson, A.L., Presto, A.A.,  
577 Subramanian, R.: Fine particle mass monitoring with low-cost sensors: corrections  
578 and long-term performance evaluation, *Aerosol Sci. Tech.*, 54, 160-174, doi:  
579 10.1080/02786826.2019.1623863, 2019.

580 Murphy, B.N., Pandis, S.N.: Exploring summertime organic aerosol formation in the  
581 eastern United States using a regional-scale budget approach and ambient  
582 measurements, *J. Geophys. Res.*, 115, D24 doi:10.1029/2010JD014418, 2010.

583 Nenes, A., Pandis, S.N., Pilinis, C.: ISORROPIA: a new thermodynamic equilibrium  
584 model for multiphase multicomponent inorganic aerosols, *Aquat. Geochem.*, 4,  
585 123–152, doi:10.1023/A:1009604003981, 1998.

586 Pan, S., Choi, Y., Roy, A., Jeon, W.: Allocating emissions to 4 km and 1 km horizontal  
587 spatial resolutions and its impact on simulated NO<sub>x</sub> and O<sub>3</sub> in Houston, TX. *Atmos.*  
588 *Environ.*, 164, 398–415, doi:10.1016/j.atmosenv.2017.06.026, 2017.

589 Robinson, E.S., Gu, P., Ye, Q., Li, H.Z., Shah, R.U., Apte, J.S., Robinson, A.L., Presto,  
590 A.A.: Restaurant Impacts on Outdoor Air Quality: Elevated Organic Aerosol Mass  
591 from Restaurant Cooking with Neighborhood-Scale Plume Extents, *Environ. Sci.*  
592 *Technol.*, 52, 9285–9294, doi:10.1021/acs.est.8b02654, 2018.

593 Stroud, C.A., Makar, P.A., Moran, M.D., Gong, W., Gong, S., Zhang, J., Hayden, K.,  
594 Mihele, C., Brook, J.R., Abbatt, J.P.D., Slowik, J.G.: Impact of model grid spacing  
595 on regional- and urban- scale air quality predictions of organic aerosol, *Atmos.*  
596 *Chem. Phys.*, 11, 3107–3118, doi:10.5194/acp-11-3107-2011, 2011.

597 Tsimpidi, A.P., Karydis, V.A., Zavala, M., Lei, W., Molina, L.T., Ulbrich, I.M., Jimenez,  
598 J.L., Pandis, S.N.: Evaluation of the volatility basis-set approach for the simulation  
599 of organic aerosol formation in the Mexico City metropolitan area, *Atmos. Chem.*  
600 *Phys.*, 10, 525–546, doi: 10.5194/acp-10-525-2010, 2010.

601 U.S. EPA: User guide: Air Quality System, Report, Research Triangle Park, N.C., available  
602 at: [https://www.epa.gov/system/files/documents/2022-08/aqs\\_user\\_guide.pdf](https://www.epa.gov/system/files/documents/2022-08/aqs_user_guide.pdf) (last  
603 access: January 2022), 2002.

604 Zakoura, M., Pandis, S.N.: Overprediction of aerosol nitrate by chemical transport models:  
605 The role of grid resolution, *Atmos. Environ.*, 187, 390–400, doi:10.1016/  
606 j.atmosenv.2018.05.066, 2018.

607 Zakoura, M., Pandis, S.N.: Improving fine aerosol nitrate predictions using a Plume-in-  
608 Grid modeling approach, *Atmos. Environ.*, 215, 116887. doi:10.1016/  
609 j.atmosenv.2019.116887, 2019.

610 Zimmerman, N., Presto, A.A., Kumar, S.P.N., Gu, J., Haurlyliuk, A., Robinson, E.S.,  
611 Robinson, A.L., Subramanian, R.: A machine learning calibration model using  
612 random forests to improve sensor performance for lower-cost air quality  
613 monitoring, *Atmos. Meas. Tech.*, 11, 291–313, doi:10.5194/amt-11-291-2018,

614            2018.  
615  
616

617 **Table 1.** Comparison of daily average high-resolution PMCAMx-v2.0 predictions with  
 618 daily EPA-CSN measurements during February and July 2017.  
 619

<b>February 2017</b>						
	<b>Sulfate</b>	<b>Nitrate</b>	<b>Ammon.</b>	<b>Elemental Carbon</b>	<b>Organic Aerosol</b>	<b>PM<sub>2.5</sub><sup>a</sup></b>
Measured Avg. ( $\mu\text{g m}^{-3}$ )	1.92	1.51	0.91	1.08	4.37	10.34
Predicted Avg. ( $\mu\text{g m}^{-3}$ )	1.70	2.90	1.62	0.94	3.68	10.52
Error ( $\mu\text{g m}^{-3}$ )	0.79	1.54	1.03	0.78	2.15	3.02
Fractional Error	0.41	0.83	0.96	0.71	0.53	0.30
Bias ( $\mu\text{g m}^{-3}$ )	-0.22	1.40	0.71	-0.14	-0.68	0.18
Fractional Bias	-0.02	0.81	0.83	-0.08	-0.01	0.05
<b>July 2017</b>						
	<b>Sulfate</b>	<b>Nitrate</b>	<b>Ammon.</b>	<b>Elemental Carbon</b>	<b>Organic Aerosol</b>	<b>PM<sub>2.5</sub><sup>a</sup></b>
Measured Avg. ( $\mu\text{g m}^{-3}$ )	2.04	0.26	0.53	0.74	4.46	11.24
Predicted Avg. ( $\mu\text{g m}^{-3}$ )	1.60	0.68	0.79	0.56	2.67	7.26
Error ( $\mu\text{g m}^{-3}$ )	1.12	0.45	0.39	0.39	2.46	4.67
Fractional Error	0.62	0.82	0.62	0.60	0.67	0.49
Bias ( $\mu\text{g m}^{-3}$ )	-0.44	0.42	0.26	-0.18	-1.85	-4.01
Fractional Bias	-0.21	0.70	0.44	-0.33	-0.47	-0.39

621 <sup>a</sup> Measurements from the regulatory EPA monitors.

622

623 **Table 2.** Comparison of daily average PMCAMx-v2.0 predicted PM<sub>2.5</sub> concentrations  
 624 during February and July 2017 with daily measurements from 17 EPA regulatory  
 625 monitors.  
 626

	<b>36 x 36 km</b>	<b>12 x 12 km</b>	<b>4 x 4 km</b>	<b>1 x 1 km</b>
<b>February 2017</b>				
Measured Avg. ( $\mu\text{g m}^{-3}$ )	10.34	10.34	10.34	10.34
Predicted Avg. ( $\mu\text{g m}^{-3}$ )	9.78	9.68	10.49	10.52
Error ( $\mu\text{g m}^{-3}$ )	3.35	3.16	3.04	3.02
Fractional Error	0.34	0.32	0.30	0.30
Bias ( $\mu\text{g m}^{-3}$ )	-0.56	-0.66	0.15	0.18
Fractional Bias	-0.09	-0.10	0.06	0.05
<b>July 2017</b>				
Measured Avg. ( $\mu\text{g m}^{-3}$ )	11.24	11.24	11.24	11.24
Predicted Avg. ( $\mu\text{g m}^{-3}$ )	6.90	6.86	7.26	7.23
Error ( $\mu\text{g m}^{-3}$ )	4.89	5.05	4.67	4.65
Fractional Error	0.53	0.53	0.49	0.48
Bias ( $\mu\text{g m}^{-3}$ )	-4.34	-4.39	-3.98	-4.01
Fractional Bias	-0.45	-0.47	-0.39	-0.39

627

628 **Table 3.** Comparison of daily average PMCAMx-v2.0 predicted PM<sub>2.5</sub> concentrations  
 629 during February and July 2017 with daily low-cost sensor (RAMP) measurements.  
 630

	<b>36 x 36 km</b>	<b>12 x 12 km</b>	<b>4 x 4 km</b>	<b>1 x 1 km</b>
<b>February 2017</b>				
Measured Avg. ( $\mu\text{g m}^{-3}$ )	11.65	11.65	11.65	11.65
Predicted Avg. ( $\mu\text{g m}^{-3}$ )	10.23	11.64	12.04	13.50
Error ( $\mu\text{g m}^{-3}$ )	4.53	4.53	4.51	5.12
Fractional Error	0.33	0.33	0.34	0.37
Bias ( $\mu\text{g m}^{-3}$ )	-1.43	-0.02	0.4	1.85
Fractional Bias	-0.02	<0.01	0.14	0.24
<b>July 2017</b>				
Measured Avg. ( $\mu\text{g m}^{-3}$ )	12.59	12.59	12.59	12.59
Predicted Avg. ( $\mu\text{g m}^{-3}$ )	7.19	7.44	8.06	8.83
Error ( $\mu\text{g m}^{-3}$ )	5.60	5.70	5.29	4.89
Fractional Error	0.51	0.51	0.46	0.42
Bias ( $\mu\text{g m}^{-3}$ )	-5.40	-5.15	-4.53	-3.76
Fractional Bias	-0.48	-0.43	-0.36	-0.27

631  
 632



633 **Table 4.** Performance of daily average predicted total PM<sub>2.5</sub> concentrations compared to  
 634 daily measurements from regulatory sites and low-cost sensors with the use of old  
 635 surrogates and new surrogates for on-road traffic and commercial cooking within the 1 x  
 636 1 km resolution grid.  
 637

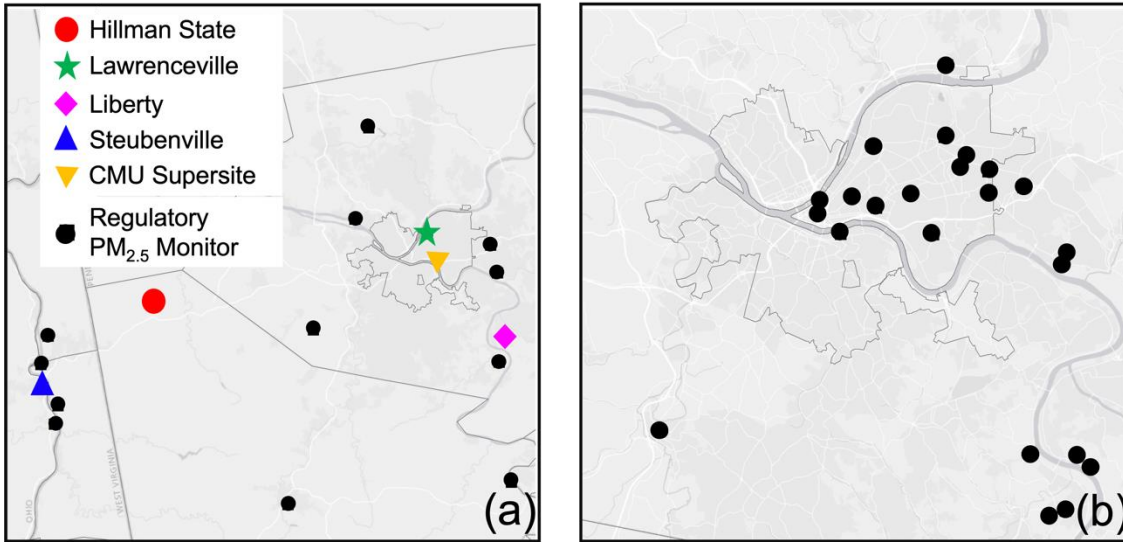
<b>February 2017</b>				
	<b>Old Surrogates</b>		<b>New Surrogates</b>	
	Regulatory network	Low-cost sensors	Regulatory network	Low-cost sensors
<b>Observed Average</b> ( $\mu\text{g m}^{-3}$ )	10.34	11.65	10.34	11.65
<b>Predicted Average</b> ( $\mu\text{g m}^{-3}$ )	10.23	11.32	10.52	13.50
<b>Error</b> ( $\mu\text{g m}^{-3}$ )	2.94	4.12	3.02	5.12
<b>Fractional Error</b>	0.29	0.31	0.30	0.37
<b>Bias</b> ( $\mu\text{g m}^{-3}$ )	-0.11	-0.33	0.18	1.85
<b>Fractional Bias</b>	-0.04	0.08	0.05	0.24

<b>July 2017</b>				
	<b>Old Surrogates</b>		<b>New Surrogates</b>	
	Regulatory network	Low-cost sensors	Regulatory network	Low-cost sensors
<b>Observed Average</b> ( $\mu\text{g m}^{-3}$ )	11.24	12.58	11.24	12.58
<b>Predicted Average</b> ( $\mu\text{g m}^{-3}$ )	7.09	7.98	7.26	8.83
<b>Error</b> ( $\mu\text{g m}^{-3}$ )	4.91	5.32	4.67	4.89
<b>Fractional Error</b>	0.51	0.47	0.49	0.42
<b>Bias</b> ( $\mu\text{g m}^{-3}$ )	-4.33	-4.61	-4.01	-3.76
<b>Fractional Bias</b>	-0.43	-0.37	-0.39	-0.27

638  
 639

640



641

642

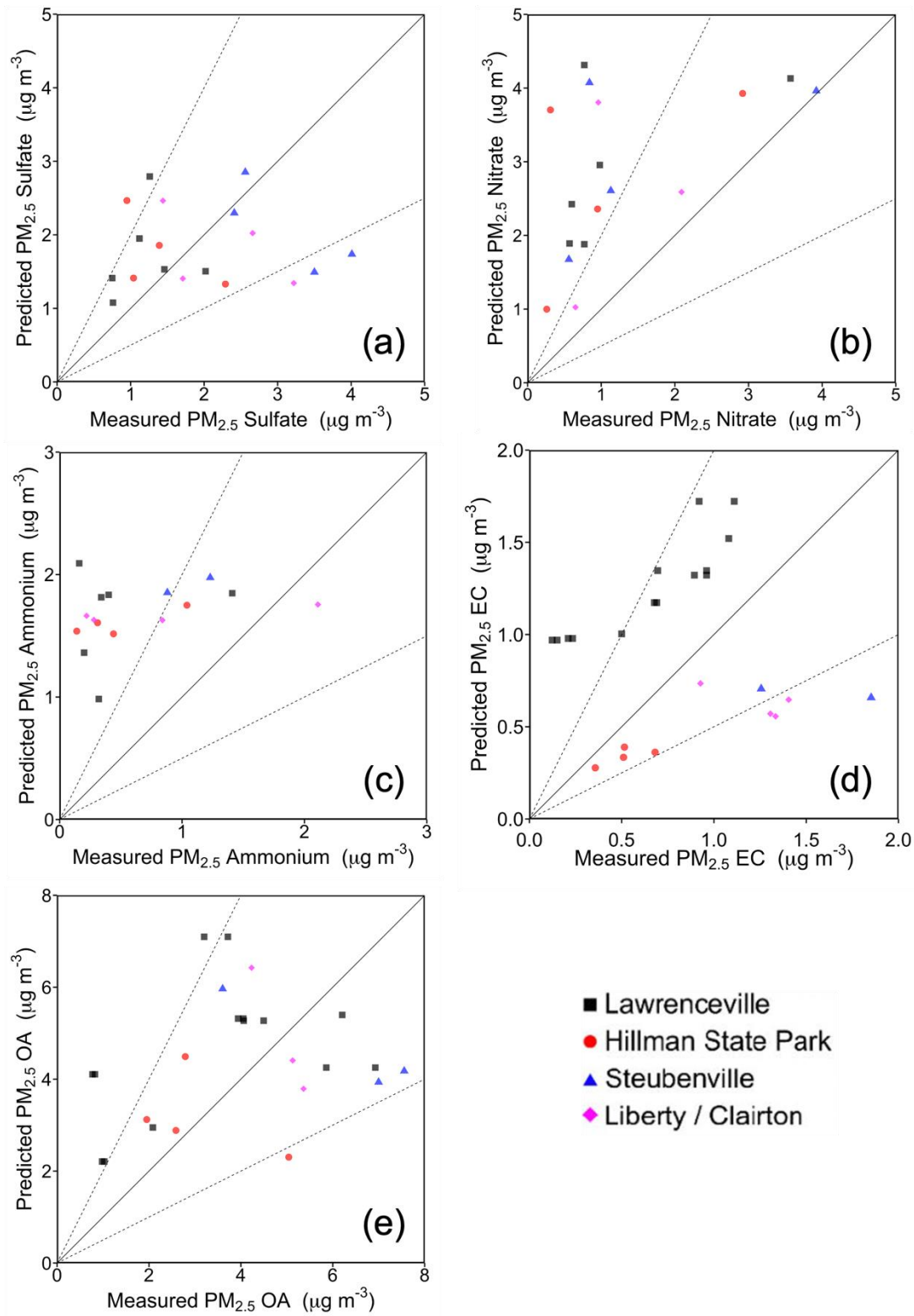
643

644

645

**Figure 1.** Monitoring sites. **(a)** Particulate matter speciation measurement sites from EPA-CSN and PM<sub>2.5</sub> regulatory monitors. The entire inner modeling domain is shown. **(b)** low-cost sensor sites. City of Pittsburgh boundaries are shown in both panels for reference.

646



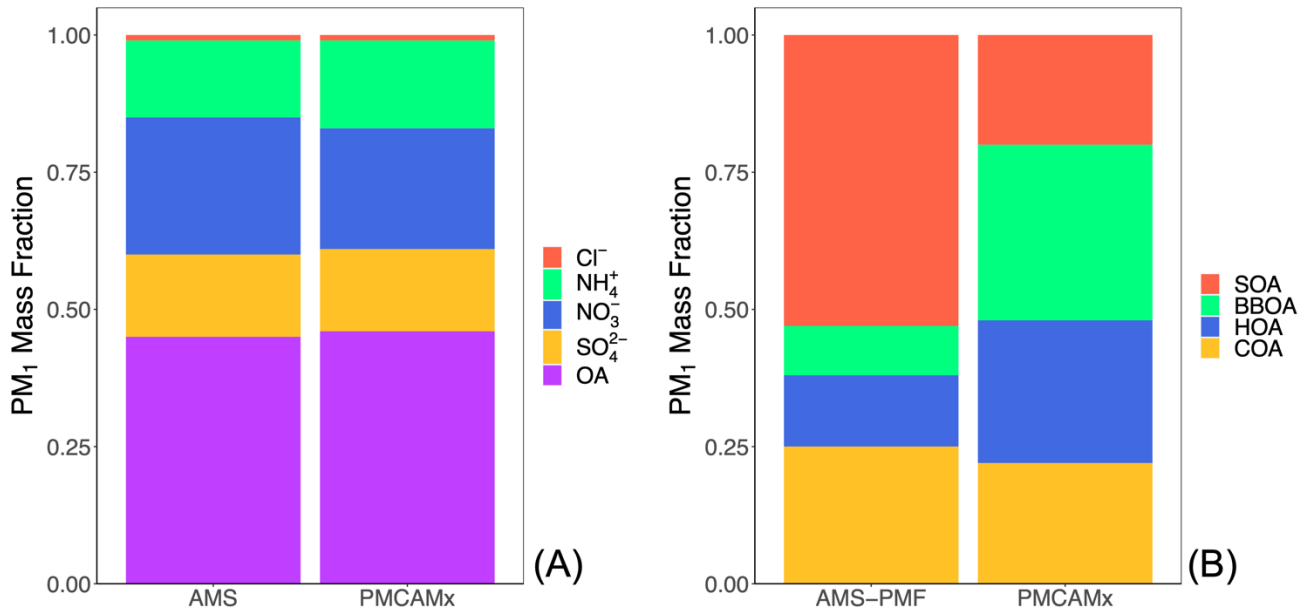
648

649

650

651

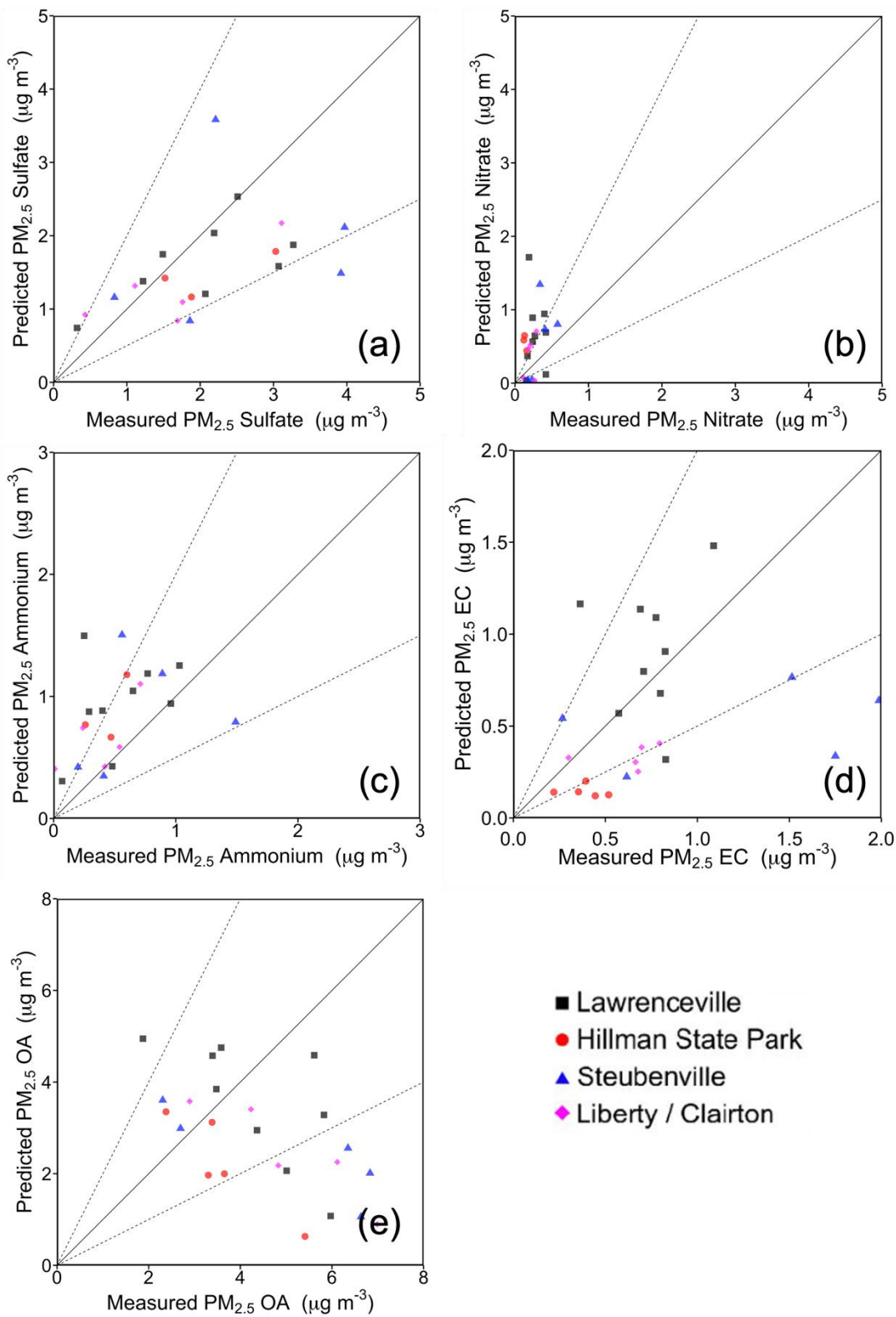
**Figure 2.** Comparison of daily average PMCAMx-v2.0 predicted concentrations of PM<sub>2.5</sub> (a) sulfate, (b) nitrate, (c) ammonium, (d) elemental carbon, and (e) organic aerosol with daily measurements from EPA-CSN sites during February 2017.



652  
653

654 **Figure 3.** (a) Comparison of PMCAMx-v2.0 predicted composition of PM<sub>1</sub> with the  
655 corresponding AMS measurements at the CMU site and (b) organic aerosol composition  
656 based on the PMF analysis of the AMS measurements and predicted composition.

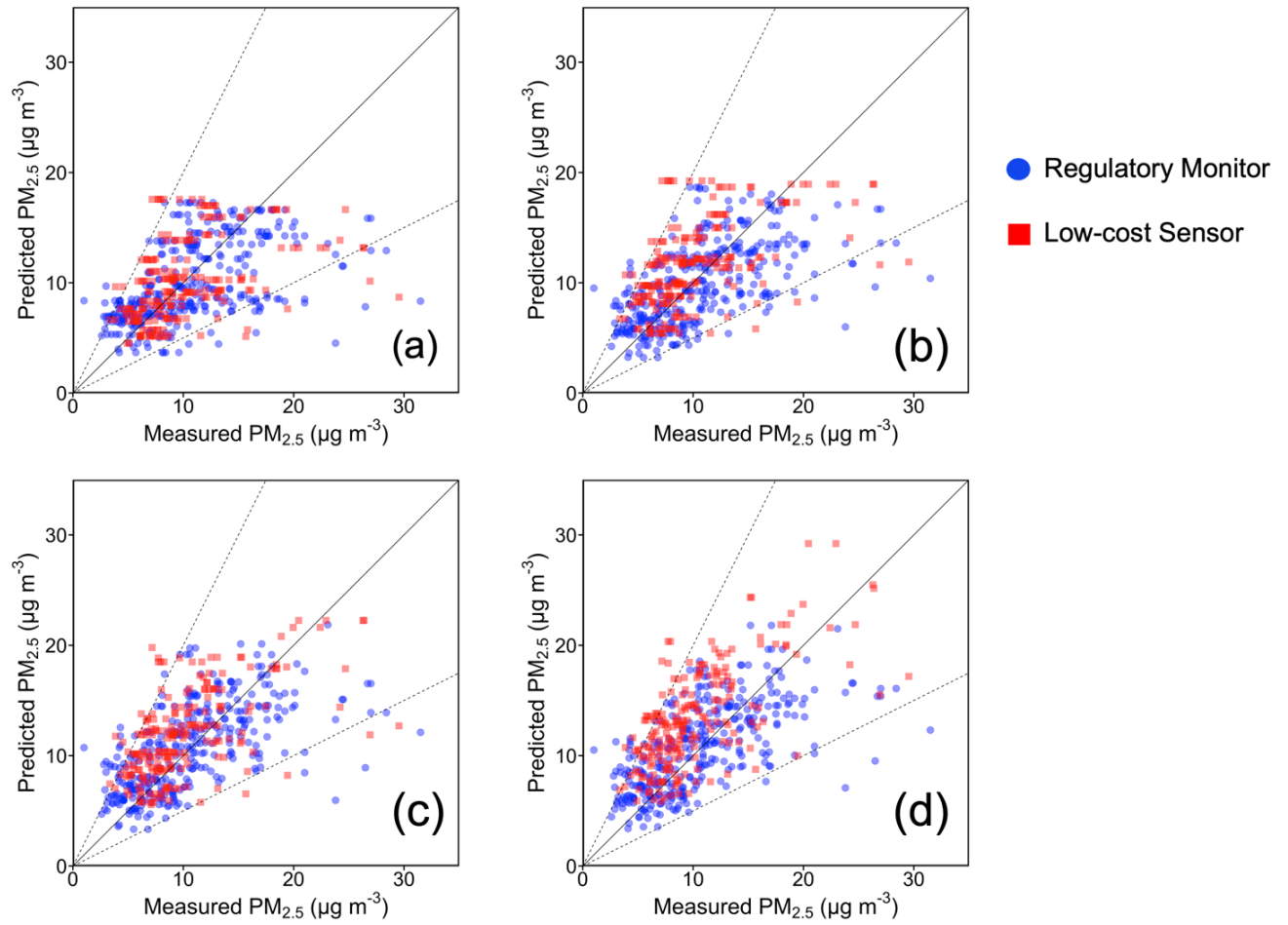
657



658  
659  
660  
661

**Figure 4.** Comparison of PMCAMx-v2.0 predicted concentrations of PM<sub>2.5</sub> (a) sulfate, (b) nitrate, (c) ammonium, (d) elemental carbon, and (e) organic aerosol with measurements from EPA-CSN sites during July 2017.

662



663

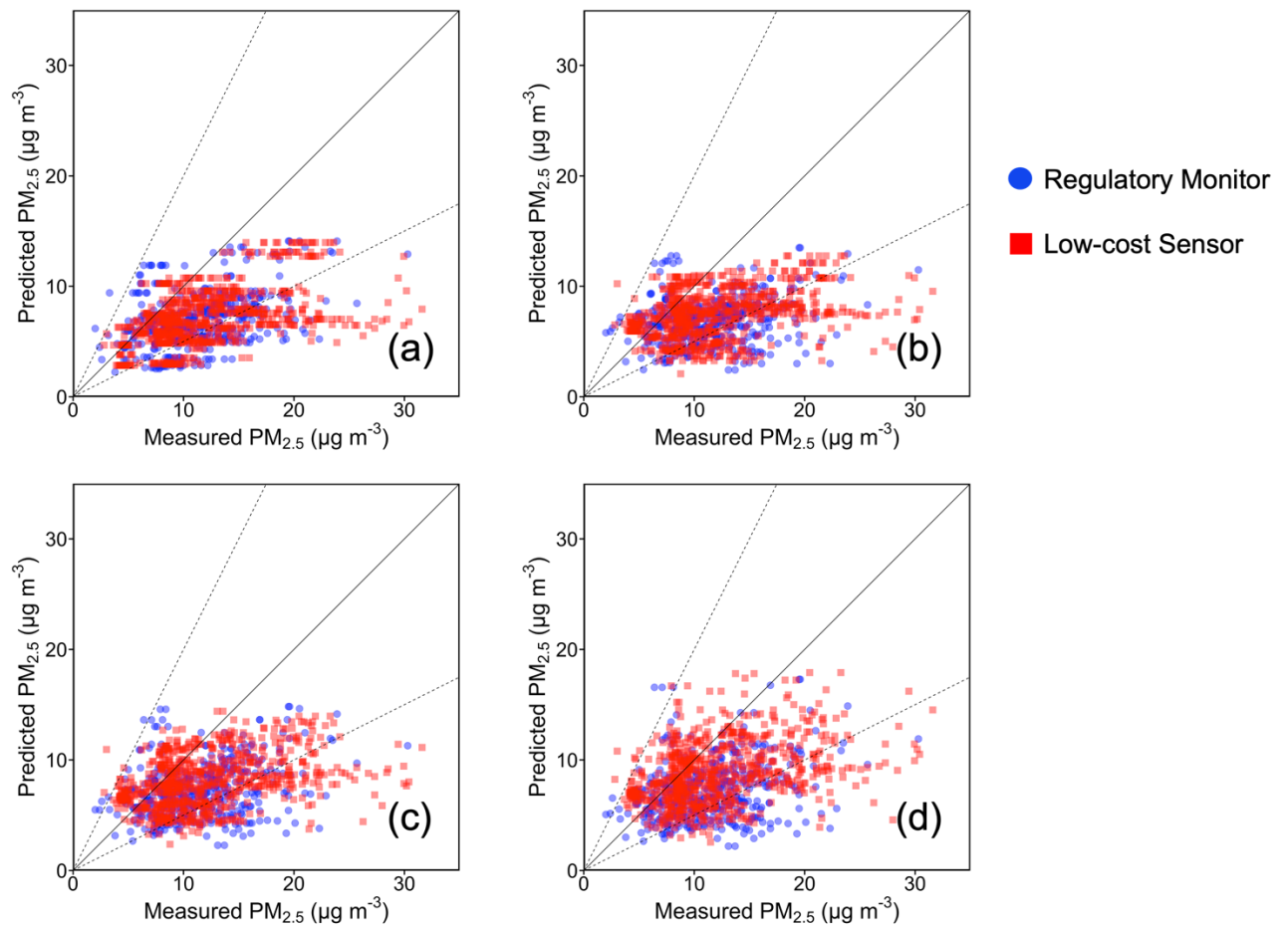
664

665 **Figure 5.** Comparison of daily average PMCAMx-v2.0 predicted concentrations of PM<sub>2.5</sub>

666 with daily regulatory measurements and daily low-cost sensor measurements at (a) 36 x

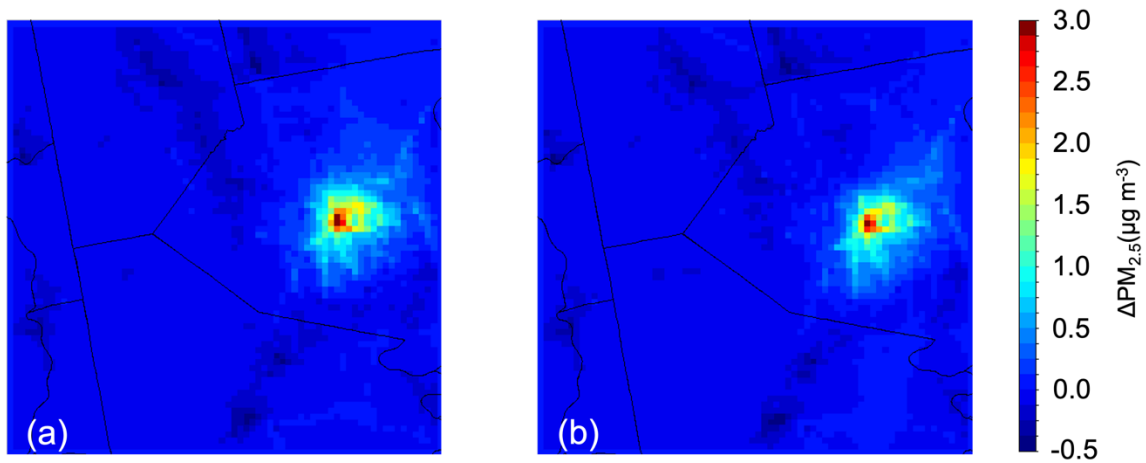
667 36, (b) 12 x 12, (c) 4 x 4, and (d) 1 x 1 km during February 2017.

668

670  
671

672 **Figure 6.** Comparison of daily average PMCAMx-v2.0 predicted concentrations of  $PM_{2.5}$   
 673 with daily regulatory measurements and daily low-cost sensor measurements at (a) 36 x  
 674 36, (b) 12 x 12, (c) 4 x 4, and (d) 1 x 1 km during July 2017.

675



676  
677  
678  
679  
680  
681

**Figure 7.** Difference between predicted monthly average  $PM_{2.5}$  mass concentration when using novel surrogates and original surrogates in (a) February 2017 and (b) July 2017 for the 1 x 1 km resolution simulation grid. A positive value indicates a higher concentration predicted with the novel surrogates.